Modeling climate change's impact on *Macrocystis pyrifera* through population dynamics

J. Alanis[1,a], L. Mossman[2,a], J. Sorenson [3,a], J.V. Molina[4], J. Rodriguez[4], S. Eikenberry[4], and C.P Ferreira[5]

[1]Sacramento State University, Sacramento CA, United States

[2]St. Olaf College, Northfield MN, United States

[3]University of Minnestoa - Twin Cities, Minneapolis MN, United States

[4]Arizona State University, Tempe AZ, United States

[5]São Paulo State University, São Paulo, Brazil

[a]Simon A. Levin Mathematical, Computational, and Modeling Sciences Center: Quantitative Research for the Life & Social Sciences Program, Arizona State University, Tempe AZ, United States

July 2021

Abstract

There is growing concern that climate change may impact the geographical distribution of foundation marine species. *Macrocystis pyrifera*, also known as giant kelp, is one such foundation species. *M. pyrifera* provides a habitat for marine animals around the world. Reproduction, growth, and survival of giant kelp is known to strongly depend on local temperature, irradiance, and pH. Giant kelp also reproduce via alternation of generations, whereby an asexual sporophyte releases haploid spores that go on to form sexed gametophytes, the females of which yield juvenile sporophytes. Differing sensitivities to temperature and other abiotic conditions in these two phases may influence population responses to climate change. Therefore, we developed a mathematical model for giant kelp population dynamics along the California coast, which includes abiotic conditions and these age-structured population dynamics. This model provided insights into how increasing sea surface temperature negatively affects *M. pyrifera* and predicts how future *M. pyrifera* populations will decrease as a result of the increasing global temperatures. The results of the model indicate that California's southern kelp populations are at a high risk of extinction by the year 2080.

Introduction

Climate Change and *Macrocystis pyrifera*

The earth's temperature fluctuates through a process called orbital variation [20]. However, humans are causing additional changes to the global climate through greenhouse gas emissions. Since the 1970's the average global temperatures have increased continuously [26]. Thus, the far reaching impacts of climate change are of major concern as global temperatures climb.

As global temperatures increase, so does sea surface temperatures [6]. Currently, it is predicted that the sea surface temperature will increase by a total of $1°C$ to $4°C$ by 2100 [4]. This increasing temperature can inflict changes to the ocean habitats, harming species residing in them. It is important to study abiotic conditions that are influenced by climate change and observe their effects on foundation species.

The influence of climate change is already seen in various foundation species such as mangroves, oak trees, coral, and more [1, 18, 25]. Climate change affects marine ecosystems through increased surface temperature, acidity, and rising sea levels [10]. One important foundation species in marine ecosystems is *Macrocystis pyrifera*, also known as giant kelp or giant bladder kelp. The close relationship between *M. pyrifera's* life cycle and oceanic abiotic factors indicates that *M. pyrifera* is impacted by climate change [11, 19].

Macrocystis pyrifera is a brown algae that resides in California, Alaska, South Africa, Australia, and New Zealand due to their cooler water temperatures [36]. Part of the Chromista biological kingdom, *M. pyrifera* is photosynthetic; however, it does not utilize a plant-like root system for nutrients. Instead, *M. pyrifera* gathers its nutrients from sunlight and the ocean's water. Instead of roots, *M. pyrifera* uses a structure similar to roots called a holdfast, or a stipe with attached floats and blades that anchors the kelp to the substrate on the seafloor. Other structural features of giant kelp include fronds which are branched sections of the organism made up of leaf like blades. The reproductive blades of *M. pyrifera* are referred to as sporophylls and are located near the holdfast. Adults continuously produce and shed both fronds and sporophylls throughout their lifetime. In one study, adult giant kelp were reported to average around 2.7 fronds at a time though they are capable of having up to 6 fronds [7]. When considering other photosynthetic organisms, *M. pyrifera's* growth rate is considered to be one of the highest. Hence, giant kelp has a quick recovery period during optimal growth conditions.

The Life Cycle of *Macrocystis pyrifera*

Through a process called alternation of generations, giant kelp reproduce asexually and sexually. Depending on favorable conditions, an adult sporophyte will generate spores via asexual reproduction within its reproductive blades, sporophylls [36]. The sporophylls contain sporangium within the blade tissue. In the nuclei of the sporangium, spores are produced through meiosis and subsequently mitotically divide two to three more times generating 16 to 32 haploid spores. Once the spores are secreted and adhere to the substrate, they

develop into female and male gametophytes which generate eggs and sperm respectively. The female gametophyte is referred to as an oogonium, and the male gametophyte is called an antheridia. When an egg is released, it remains anchored to the female gametophyte while sperm are motile. Once the sperm comes into contact and fertilizes the egg, the egg becomes a zygote which grows from a juvenile sporophyte to an adult sporophyte. Here, it is assumed that juvenile sporophytes are reproductively immature and the transition to adult sporophytes coincides with reproductive maturity when juveniles are approximately 1 meter in length. The known life expectancy of *M. pyrifera* can reach up to 9 years. However, it typically lives within the range of 4 to 7 years, and even less in the presence of severe disturbances such as storms or heat waves such as El Niños [16]. Overall, throughout its adult stage, giant kelp will continuously release spores, and the reproductive cycle will continue on until death. See Figure 1 for a visualization of *M. pyrifera's* life cycle.

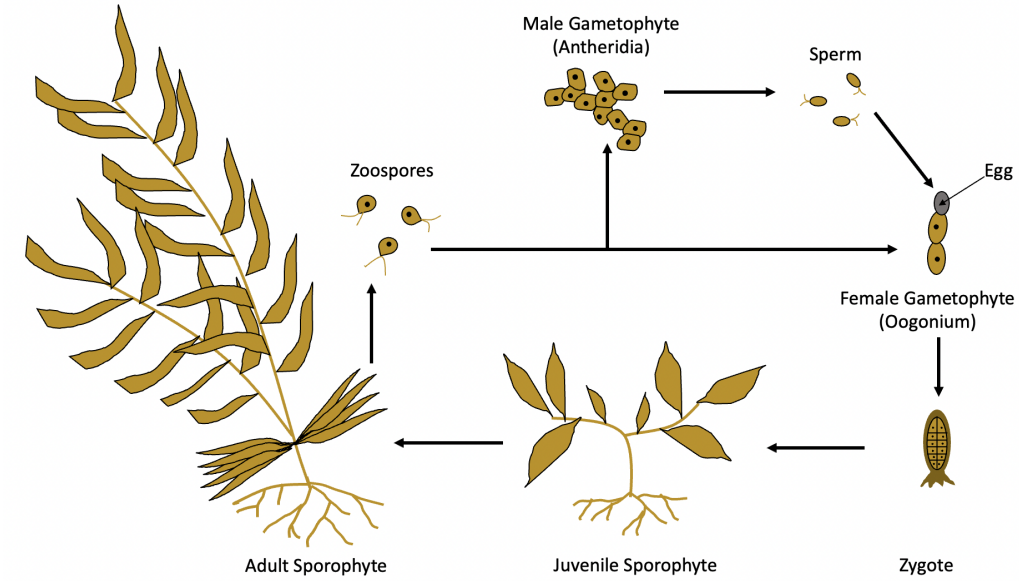

Figure 1: Illustration depicting the life cycle of *Macrocystis pyrifera*.

Abiotic Growth Conditions

Giant kelp growth and reproduction is sensitive to abiotic factors including temperature, nutrient availability, and irradiance. In order to achieve optimal growth, giant kelp must grow in temperatures between 4 °C and 20 °C [36]. In these conditions, *M. pyrifera* grows an average of 10 to 35 cm a day.

In order to form its canopy, adult *M. pyrifera* can grow to surface water heights making them more suceptable to surface water temperature fluctuations than other organisms in the kelp bed. In an experiment that used untethered or floating sporophytes, temperatures higher than 20 °C were reported to cause temperature-related damage to the organism [34]. Specifically, species in California were damaged at temperatures greater than 24 °C. Symptoms of temperature damage included brittleness and pigment loss which appear one week

after exposure to high temperatures. Another study reported that during a heat wave above 24 °C juvenile populations experienced a minimum of 80% juvenile mortality within a 5 day period [8]. The micro stages of the cycle is also negatively impacted by fluctuating temperatures. For example, gametophyte populations had a negative response to temperature with regards to egg production [19].

Another important abiotic factor is nutrient availability, which has a strong direct influence on the growth and reproduction of *M. pyrifera* [36]. In support, Buschmann, *et al.* researched nutrients' and temperatures' effect on giant kelp [7]. In this study, giant kelp were placed at two temperatures: 12 °C and 18 °C and with or without nitrogen. Afterward, it was noted that higher temperatures reduced the growth rate of the sporophytes, but nitrogen treatments also had a significant influence on the sporophytes. Also, lower temperatures combined with the nitrogen treatment showed significant increases in growth rate and surface area.

Irradiance, the quantity of light at various water levels, is another factor that impacts *M. pyrifera's* growth. In a previous study, juvenile sporophytes were transplanted to depths of 3 and 10 meters in a water column [38]. The results indicated that juvenile sporophytes at 3 meters showed a significant decrease in photosynthetic efficiency while respiration rates increased, impacting kelp growth.

Overall, there are many abiotic factors that have a significant impact on the growth, recruitment, and survival of *M. pyrifera*. Thus, by simulating the interdependence between abiotic factors and the *M pyrifera* life cycle, we can illustrate how *M. pyrifera* reacts under climate changes conditions such as rising temperatures.

Previous Works

In 1989, Nisbet and Bence created a population dynamics model of adult *M. pyrifera* through delayed differential equations [27]. The model considers only the adult population while the delay refers to the time spent in the other life stages (from zoospores to adult). In this model, strict threshold values (for temperature and irradiance) are imposed on the juvenile recruitment rate such that nonoptimal temperatures and irradiance results in no new adult sporophytes. Through simulations, they study how adult *M. pyrifera* population density is affected by temperature and irradiance variations. With the addition of a stochastic term to the juvenile recruitment rate, which accounts for other biological conditions not considered in the model, they successfully replicated in situ *M. pyrifera* population dynamics [27].

Detmer *et, al* created an ODE age-structured system that incorporated the dynamics of understory macroalgae, sessile invertebrates, gametophyte *M. pyrifera*, juvenile *M. pyrifera*, and adult *M. pyrifera* in response to storm wave disturbances [12]. Studying *M. pyrifera's* impact on the benthic community members, the researchers found that disturbance-driven fluctuations in the abundance *M. pyrifera* significantly effects resource competition within the benthic community.

Building on previous mathematical models [12, 27], we focus on the dynamics of gametophytes, juvenile, and adult giant kelp as temperature and irradiance fluctuates. For that, a non-autonomous ODE age-structure model will be proposed. Uniquely, this model uses temperature data and density dependent irradiance to

construct different scenarios where the population's growth is continuously affected by these abiotic factors. Using this model we will be able to predict the abundance of giant kelp off the coast of California and analyze how abiotic factors impact *M. pyrifera's* life stages.

Methods

Model Assumptions

In the context of the system, specific assumptions were made about the *M. pyrifera's* life cycle in order to model how the dynamics affects the life stages of *M. pyrifera's* within a kelp bed. We assumed that our population resided in a single average sized kelp bed off the coast of California. Kelp beds are oceanic regions along part of the world's coastline that hold large densities of kelp. Our kelp bed was also closed which eliminates any migration to and from surrounding kelp beds. Thus, migration is not considered in our model.

We also exclude the spores population from the age structure. Adult sporophytes can produce as many as 500,000 spores per hour [2], resulting in a high spore concentration within the kelp bed. Thus, excluding the spore population eliminates unnecessary complexity without impacting the population dynamics. The model does not take into consideration that the dispersion of spores is uneven or that the rate of spores that reach the outer parts of the kelp bed is reduced. The *M. pyrifera* population with in the kelp bed is considered to be homogenous.

Another simplification of the model is through the exclusion of the male gametophyte population. It is the female gametophytes which develop a holdfast. Hence, it is the female gametophytes who eventually transition into the juvenile stage. Since the sex ratio for an individual gametophyte is 50:50, only half of the population was included [36]. We also assume that female gametophytes have no influences on the competition term between juveniles and adults. In terms of size, the gametophyte holdfast is insignificant compared to the juvenile and adult holdfasts [36]. This assumption is implemented in the gametophyte competition term where only the density of adults and juveniles' population affects the gametophyte production.

We presume that the abiotic factor temperature strongly influences juvenile and adult death, and affects adult recruitment via the growth rate of juveniles [15]. We also assume that the abiotic factor irradiance strongly influences the recruitment rate of juvenile sporophytes. [38].

Implementing Abiotic Factors

Previous studies indicated that the growth rate of gametophytes is impacted by ocean bottom irradiance [22]. The units of irradiance are $\frac{mol}{m^2 s}$ where moles refers to moles of photons, or light particles. Given the correlation between adult giant kelp density and the quantity of irradiance reaching the substrate, the juvenile

recruitment rate, $\gamma(L_B(\hat{A}(t)))$, depends on irradiance (which depends on adult density) and is of the form:

$$\gamma(L_B(\hat{A}(t))) = r_G \times L_B(\hat{A}(t)) \tag{1}$$

Then, $\hat{A}(t)$ is the density of the giant kelp at time t calculated by $\hat{A}(t) = \frac{A(t)}{\theta}$. A is the adult population and θ is the average kelp bed area. Additionally, r_G is the recruitment rate of juveniles per bottom irradiance. Then, $L_B(\hat{A}(t))$ is the bottom irradiance dependent on adult density which follows the Lambert-Beer law and is of the form:

$$L_B(\hat{A}(t)) = L_S \times e^{-k_1 \times \hat{A}(t)} \tag{2}$$

where k_1 is the attenuation coefficient and L_S is the average daily surface irradiance [12]. When there are no adults, ($\hat{A}(t) = 0$) then the juvenile recruitment rate is equivalent to $r_G \times L_S$. See Table 1 for parameter values.

The adult recruitment rate, $\sigma(GR)$, is a function of the growth rate, GR. From lab experiments, we know that there is a quadratic relationship between temperature and relative growth rate [15]. The quadratic $GR(T(t))$, is a function of temperature at time t.

$$GR(T(t)) = \begin{cases} -\dfrac{(T(t)-2)(T(t)-26)}{36.92 \times 100}, & 2 < x < 26. \\ 0, & x \leq 2,\ x \geq 26. \end{cases} \tag{3}$$

The values 36.92 and 100 in the function are both scalars that are used to create a maximum growth rate of 0.039 at 14°C. If $GR(T(t)) \leq 0$ at time t, then we assume that $\sigma(GR(T(t)))$ is 0, since a negative growth has no applicable biological meaning. Otherwise if $GR(T(t))$ is positive, we can solve for the time x it take for the juvenile to become an adult using an exponential growth function dependent on the relative growth rate. The time x is determined by solving for $1 = 0.075 \times e^{GR(T(t))x}$ where 0.075 is the average initial length of a juvenile sporophyte and 1 is the length threshold from juvenile to adult in meters [36]. Finally, $\sigma(GR(T(t)))$, the rate at which juveniles become adults is:

$$\sigma(GR(T(t))) = \begin{cases} \frac{1}{x}, & GR(T(t)) \neq 0. \\ 0, & GR(T(t)) = 0. \end{cases} \tag{4}$$

The juvenile death rate, $\delta_J(T(t))$, is a monotonic increasing hill function of the form:

$$\delta_J(T(t)) = (\delta_{Jmax} - \delta_{Jmin}) \frac{(T(t))^{10}}{\zeta_J^{10} + (T(t))^{10}} + \delta_{Jmin} \tag{5}$$

Within the range of temperatures we studied, the death rate $\delta_J(T(t))$ must remain positive. The maximum death rate δ_{Jmax} occurs at high temperatures while the minimum death rate δ_{Jmin} occurs at low temperatures.

To ensure $\delta_J(T(t)) > 0$ for all time, $\delta_{Jmax} > \delta_{Jmin}$. As temperatures exceed ζ_J, juveniles will begin to experience higher levels of stress and mortality. Hence, $\delta_J(T(t))$ is half the maximal death when the temperature is equal to ζ_J. A power of 10 was utilized to sufficiently increase the the steepness of the curve, in order to simulate the large increase in death near the threshold and to maintain low death rates within the optimal temperature range.

Similarly, the adult death rate, δ_A, is also monotonic increasing hill function of the form:

$$\delta_A(T(t)) = (\delta_{Amax} - \delta_{Amin}) \frac{(T(t))^{10}}{\zeta_A^{10} + (T(t))^{10}} + \delta_{Amin} \tag{6}$$

The reasoning for this function is the same as for $\delta_J(T(t))$ except that δ_{Amax}, the death rate at high temperatures, and δ_{Amin}, the death rate in optimal temperature ranges, are different values. In this hill function, ζ_A has the same value as juveniles. See Table 1 for parameter values.

Table 1: Model's variable and parameters description with their units.

Variable	**Description**		**Unit**	**References**
T	Temperature.		°C	
$\hat{A}$	Density of *Macrocystis Pyrifera.*		$\frac{adult}{m^2}$	
Parameter	**Description**	**Value**	**Unit**	**References**
$GR(T(t))$	Juvenile growth rate.		$\frac{1}{day}$	[30]
θ	Average kelp bed area.	34,254	m^2	[30]
k_1	Attenuation coefficient.	6.12	$\frac{m^2}{adult}$	[12]
L_S	Average daily surface irradiance.	1,000	$\frac{mol}{m^2 s}$	[13]
$L_B(\hat{A}(t))$	Bottom irradiance.		$\frac{mol}{m^2 s}$	[13]
r_G	Juvenile recruitment rate per bottom irradiance.	5×10^{-5}	$\frac{m^2 \cdot s}{mol \cdot day}$	[13]
δ_{Amin}	Minimum per capita adult death rate.	0.0027	$\frac{1}{day}$	[36]
δ_{Amax}	Maximum per capita adult death rate.	0.0045	$\frac{1}{day}$	[23]
δ_{Jmin}	Minimum per capita juvenile death rate.	0.01	$\frac{1}{day}$	[36]
δ_{Jmax}	Maximum per capita juvenile death rate.	0.1640	$\frac{1}{day}$	[8]
ζ_A	Temperature at half maximal death rate for adults.	24	°C	[9]
ζ_J	Temperature at half maximal death rate for juveniles.	24	°C	[9]

Model Description

Based on our assumptions, the non-autonomous age-structured population model considers female gametophytes (G), juvenile (J) sporophytes, and adult sporophytes (A).

In our model, the kelp population exists in a closed kelp bed. In the kelp bed, adults continuously release

spores into the environment. Even though this life stage is not included in the population dynamics due to their relative abundance, it is understood that these spores settle into the substrate and grow into gametophytes. For the female gametophyte population, G, we assumed that $0.5 \times \beta$ gametophytes are produced per adult A per day. Note the 1:1 sex ratio [33]. The competition term, $\left(1 - \frac{0.085 \times J + 0.915 \times A}{K}\right)$, accounts for each gametophyte competing with juvenile and adult holdfasts.

The female gametophytes, G, die at a rate δ_G and grow to juvenile sporophytes, J, at a rate $\gamma(L_B(\hat{A}(t)))$. A sporophyte remains in the juvenile stage while it is less than a meter in length. The juvenile is recruited to the adult sporophyte state, A, at a rate $\sigma(GR(T(t)))$ and dies at a rate $\delta_J(T(t))$. In the adult stage, the adult sporophytes die at a rate $\delta_A(T(t))$. Table 2 futher details the parameter values and variables. The dynamical system that captures the described behavior is:

$$\frac{dG}{dt} = 0.5 \times \beta \times A \times \left(1 - \frac{0.085 \times J + 0.915 \times A}{K}\right) - \gamma(L_B(\hat{A}(t))) \times G - \delta_G \times G \tag{7}$$

$$\frac{dJ}{dt} = -\sigma(GR(T(t))) \times J + \gamma(L_B(\hat{A}(t))) \times G - \delta_J(T(t)) \times J \tag{8}$$

$$\frac{dA}{dt} = \sigma(GR(T(t))) \times J - \delta_A(T(t)) \times A \tag{9}$$

Table 2: Model's variable and parameters description with their units.

Variable	**Description**		**Unit**	**References**
A	Adult sporophyte ($\geq 1m$).		individual	[17]
J	Juvenile sporophyte ($< 1m$).		individual	[17]
G	Female gametophyte.		individual	
Parameter	**Description**	**Value**	**Unit**	**References**
β	Gametophyte production rate per adult.	0.185	$\frac{1}{day}$	[12, 39]
$\gamma(L_B(\hat{A}(t)))$	Recruitment rate from gametophyte to juvenile.		$\frac{1}{day}$	
$\sigma(GR(T(t)))$	Recruitment rate from juvenile to adult.		$\frac{1}{day}$	
δ_G	Per capita gametophyte death rate.	0.3750	$\frac{1}{day}$	[9]
$\delta_J(T(t))$	Per capita juvenile death rate.		$\frac{1}{day}$	
$\delta_A(T(t))$	Per capita adult death rate.		$\frac{1}{day}$	
K	Juvenile and adult carrying capacity.	126,867	individuals	[29]

Simulation Protocol

The simulations were performed using Matlab (Version R2021a). The appendix contains the entire source code for future reference. To analyze the impacts of temperature on the adult, juvenile, and gametophyte populations of *M. pyrifera*, we simulated temperature data and ran the model for six years (unless otherwise

stated).

We observed how different kelp populations varied based on location. Using six separate locations along California's coastline (see Figure 2), the population of giant kelp was analyzed with shore station water surface temperature data over a 15 year interval [31, 24]. Missing data points were parsed out and were not included in the final simulation. The locations studied were San Clemente, Farallons, La Jolla, Mendocino, Trinidad and Santa Barbara. Simulations began with an initial condition of 2500 gametophytes, 2000 juveniles, and 5000 adults starting at the year 2005. The simulation continued until it reached 2020. Finally, the results for the first 5 years were excluded from the final observations to allow time for the populations to adjust to each location.

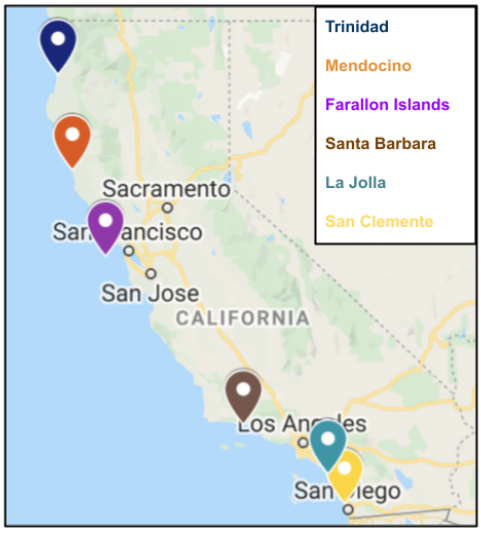

Figure 2: Map of compared locations along the coast of California.

Generating sea surface temperature based on San Clemente, CA's temperature profile and the prediction that SST will increase by a maximum of 4 °C by 2100 [4], we simulated how global warming will impact *M. pyrifera* populations. San Clemente's interannual temperature varied by an average of 12.9 °C with a mean temperature of 17.6 °C. Thus, the following equation for temperature was derived:

$$T = 6.45 \sin\left(\frac{2\pi t}{365}\right) + 1.3 \times 10^{-4} t + 17.6$$

where t is time in days and T is temperature in °C.

Model Trait Comparison

While other models either exclude the gametophyte population or group female and male gametophytes populations as one class, our model restricts the gametophytes population to only females since they give rise to the juvenile sporophytes. Considering that the eggs of the females remain anchored to the gametophyte,

they are also easier to keep track of. Additionally, unlike in Nisbet's model [27], we included parameters influenced by temperature as a continuous function rather than as a switch function. The adult recruitment σ is a function of growth rate which is a function of temperature over time. *In vivo*, recruitment of juveniles into adults is lowered during extreme temperatures, but ultimately some giant kelp will survive [14]. To reflect this also included death rates which were continuous functions of temperature and time. In addition, our function can be adjusted to model historical temperature data or it can run for an extended amount of time in the future to capture the effects of climate change. Another novel feature is the ability to include real daily surface temperature data or a continuous function of temperature from various locations. Lastly, the juvenile recruitment rate γ, which is a function of irradiance, is commonly used when modeling *M. pyrifera*. The function was kept continuous such as in Detmer's model [12], but the rate was adjusted using the average kelp bed size and experimental data on the timing of gametogenesis.

Results

The following sections include an analysis on the stability of our model and different simulations. Simulations were run using constant temperatures, different location temperatures, and predicted future temperatures.

Stability Analysis

Under the assumption of constant parameters, we analyzed the stability of the system's equilibria. For this we solved the system

$$\begin{aligned} 0 &= \frac{dG}{dt} \\ 0 &= \frac{dJ}{dt} \\ 0 &= \frac{dA}{dt} \end{aligned}$$

which resulted in two equilibrium: a trivial equilibrium at $G^* = 0, J^* = 0, A^* = 0$ and a nontrivial equilibrium:

$$\begin{aligned} G^* &= \frac{200K\delta_A(\delta_J+\sigma)(\delta_A\delta_G(-2\delta_J-2\sigma)+\gamma(-2\delta_A\delta_J+\beta\sigma-2\delta_A\sigma))}{\beta\gamma^2\sigma(17\delta_A+183\sigma)}, \\ J^* &= \frac{200K\delta_A(\delta_A\delta_G(-2\delta_J-2\sigma)+\gamma(-2\delta_A\delta_J+\beta\sigma-2\delta_A\sigma))}{\beta\gamma\sigma(17\delta_A+183\sigma)}, \\ A^* &= \frac{K(\delta_A\delta_G(-400\delta_J-400\sigma)+\gamma(-400\delta_A\delta_J+200\beta\sigma-400\delta_A\sigma))}{\beta\gamma(17\delta_A+183\sigma)} \end{aligned}$$

In order, for our populations to coexist, the nontrivial equilibrium $G^*, J^*, A^* > 0$. For $G^* > 0$, then we get the

expression:

$$0 < \delta_A \delta_G(-2\delta_J - 2\sigma) + \gamma(-2\delta_A \delta_J + \beta\sigma - 2\delta_A \sigma)$$

From this we get a threshold of

$$1 < \frac{\beta\gamma\sigma}{\delta_A(\gamma + \delta_G)(\delta_J + \sigma)}$$

We then assigned the threshold expression the value R_1 where

$$R_1 = \frac{\beta\gamma\sigma}{2\delta_A(\gamma + \delta_G)(\delta_J + \sigma)}$$

The threshold for J^* and A^* is the same as for G^* which that $R_1 > 1$.

To analyze the stability of the model we first found the Jacobian as

$$J = \begin{bmatrix} \frac{\partial \dot{G}}{\partial G} & \frac{\partial \dot{G}}{\partial J} & \frac{\partial \dot{G}}{\partial A} \\ \frac{\partial \dot{J}}{\partial G} & \frac{\partial \dot{J}}{\partial J} & \frac{\partial \dot{J}}{\partial A} \\ \frac{\partial \dot{A}}{\partial G} & \frac{\partial \dot{A}}{\partial J} & \frac{\partial \dot{A}}{\partial A} \end{bmatrix} = \begin{bmatrix} \gamma - \delta_G & \frac{-0.0425A\beta}{K} & 0.5\left(1 - \frac{0.915A + 0.085J}{K}\right)\beta - \frac{0.4575A\beta}{K} \\ \gamma & \delta_J - \sigma & 0 \\ 0 & \sigma & \delta_A \end{bmatrix}$$

To analyze the trivial equilibrium, we utilized the Routh Hurwitz Criteron for the general parameter case of stability. In addition, we analyzed the stability of parameters at two different temperatures. First we define a_1, a_2, a_3 as:

$$a_1 = -\text{tr}(J)$$

$$a_2 = \det\begin{bmatrix} a_{11} & a_{12} \\ a_{21} & a_{22} \end{bmatrix} + \det\begin{bmatrix} a_{11} & a_{13} \\ a_{31} & a_{33} \end{bmatrix} + \det\begin{bmatrix} a_{22} & a_{23} \\ a_{32} & a_{33} \end{bmatrix}$$

$$a_3 = -\det(J)$$

For the equilibrium to be stable the following three criteria must be met:

1. $a_1 > 0$
2. $a_3 > 0$
3. $a_1 a_2 > a_3$

To analyze the stability of the nontrivial equilibrium, we first evaluated the Jacobian at $G^* = 0, J^* = 0, A^* = 0$.

$$J(0,0,0) = \begin{bmatrix} \gamma - \delta_G & 0 & 0.5\beta \\ \gamma & \delta_J - \sigma & 0 \\ 0 & \sigma & \delta_A \end{bmatrix}$$

Following the above definitions here are a_1, a_2, a_3 and $a_1 \times a_2$:

$$a_1 = \gamma + \delta_A + \delta_G + \delta_J + \sigma$$
$$a_2 = \delta_G\delta_J + \delta_G\sigma + \gamma(\delta_A + \delta_J\sigma) + \delta_A(\delta_G + \delta_J\sigma)$$
$$a_3 = -0.5\beta\gamma\sigma + \gamma\delta_A(\delta_J + \sigma) + \delta_A\delta_G(\delta_J + \sigma)$$
$$a_1 \times a_2 = (\gamma + \delta_A + \delta_G + \delta_J + \sigma)(\delta_G\delta_J + \delta_G\sigma + \gamma(\delta_A + \delta_J + \sigma) + \delta_A(\delta_G + \delta_J + \sigma))$$

First note that $\gamma, \delta_A, \delta_G, \delta_J$, and σ are positive rates so criterion 1 is met. For criterion 2 to be met, we rearranged the expression and substituted R_1 into it.

$$1 < \frac{2\delta_A(\gamma + \delta_G)(\delta_J + \sigma)}{\beta\gamma\sigma}$$
$$1 < \frac{1}{R_1}$$

Thus, for criterion 2 to be met:

$$R_1 < 1$$

Lastly, for criterion 3 to hold, the expression can be rewritten and substituted as

$$1 < \frac{2a_1a_2 + \beta\gamma\sigma}{2\delta_A(\gamma + \delta_G)(\delta_J + \sigma)}$$
$$1 < \frac{a_1a_2}{\delta_A(\gamma + \delta_G)(\delta_J + \sigma)} + R_1$$

Finally, criterion 3 will hold if

$$R_1 > 1 - \left(\frac{a_1a_2}{\delta_A(\gamma + \delta_G)(\delta_J + \sigma)}\right)$$

Thus, for a general case, the trivial equilibrium is stable when

$$1 - \left(\frac{a_1a_2}{\delta_A(\gamma + \delta_G)(\delta_J + \sigma)}\right) < R_1 < 1$$

Since condition two and three depend on parameters that vary significantly at various temperatures, two

temperature scenarios are analyzed: the optimal temperature of 14°C and an non-optimal temperature of 24°C. At a constant 24°C, $\sigma = 0.0046, \delta_A = 0.0036, \delta_J = 0.087, \gamma = 0.05$. Using these parameters we find that $a_1 = 0.52, a_2 = 0.041, a_3 = 1.2 \times 10^{-4}, a_1 a_2 = 0.021$. All the conditions are met so the extinction equilibrium is stable when there is a constant temperature of 24°C. At a constant 14°C, $\sigma = 0.0151, \delta_A = 0.0027, \delta_J = 0.0107, \gamma = 0.0403$. Using these parameters we find that $a_1 = 0.44, a_2 = 0.012, a_3 = -2.7 \times 10^{-5}, a_1 a_2 = 5.3 \times 10^{-3}$. Condition two is not met so the extinction equilibrium is unstable when there is a constant temperature of 14°C.

To analyze the stability of the coexistence equilibrium,

$$G^* = \frac{200K\delta_A(\delta_J + \sigma)(\delta_A\delta_G(-2\delta_J - 2\sigma) + \gamma(-2\delta_A\delta_J + \beta\sigma - 2\delta_A\sigma))}{\beta\gamma^2\sigma(17\delta_A + 183\sigma)},$$
$$J^* = \frac{200K\delta_A(\delta_A\delta_G(-2\delta_J - 2\sigma) + \gamma(-2\delta_A\delta_J + \beta\sigma - 2\delta_A\sigma))}{\beta\gamma\sigma(17\delta_A + 183\sigma)},$$
$$A^* = \frac{K\delta_A\delta_G(-400\delta_J - 400\sigma) + \gamma(-400\delta_A\delta_J + 200\beta\sigma - 400\delta_A\sigma)}{\beta\gamma(17\delta_A + 183\sigma)}$$

we first evaluated the Jacobian. See Appendix A.1 for the full Jacobian and a_1, a_2, a_3 and $a_1 \times a_2$. Note that $\gamma, \delta_A, \delta_G, \delta_J$, and σ are positive rates, so condition one is met. See appendix A.1 for an analysis of when condition 2 and 3 are met.

Since condition two and three depend on parameters that vary significantly at various temperatures, two temperature scenarios are analyzed: optimal temperature of 14°C and an non-optimal temperature of 24°C. At a constant 24°C, $\sigma = 0.0046, \delta_A = 0.0036, \delta_J = 0.087, \gamma = 0.05$. Using these parameters we find that $a_1 = 0.52, a_2 = 0.039, a_3 = -1.2 \times 10^{-4}, a_1 a_2 = 0.02$. Condition 2 is not met so the coexistence equilibrium is unstable when there is a constant temperature of 24°C. At a constant 14°C, $\sigma = 0.0151, \delta_A = 0.0027, \delta_J = 0.0107, \gamma = 0.0403$. Using these parameters we find that $a_1 = 0.44, a_2 = 0.012, a_3 = 2.7 \times 10^{-5}, a_1 a_2 = 5.3 \times 10^{-3}$. All the conditions are met so the coexistence equilibrium is stable when there is a constant temperature of 14°C.

Relationship Between Temperature and *M. pyrifera*

To analyze temperature's impact on *M. pyrifera*, the model ran for 8 years at a constant temperature. Once reaching a constant size, the population size at the temperature was recorded. Figure 3 illustrates the gametophytes, juvenile, and adult population size at discrete temperature steps.

The resulting adult and gametophyte population size follows a quadratic curve, with a maximum population size at 14 °C. Alternatively, two factors contribute to the maximum juvenile population occuring at 5 °C: a larger juvenile recruitment rate, $\gamma(L_B)$ and smaller juvenile death rate, $\delta_J(T(t))$. At low temperatures, the relatively low adult density, $\hat{A}$ results in a larger juvenile recruitment rate, which is a function of $\hat{A}$. Additionally, at low temperatures, $\delta_J(T(t))$ is extremely close the δ_{Jmin} by definition of a Hill function.

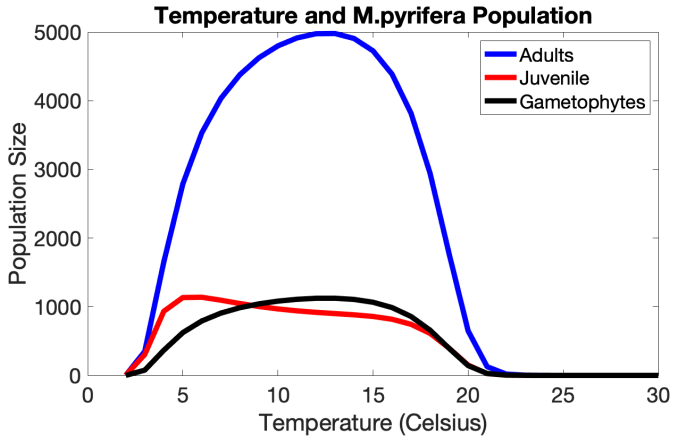

Figure 3: Population size after 6 years at various constant temperatures.

To add yearly temporal variation, a total 5 °C variation was considered at each baseline temperature (ranging 2 to 30 °C).

$$T = 2.5 \sin\left(\frac{2\pi t}{365}\right) + T_{base}$$

Where T is the daily temperature, t is the day, and T_{base} is the baseline temperature for each simulation. Figure 4 illustrates the effect of small interannual temporal variations for each population.

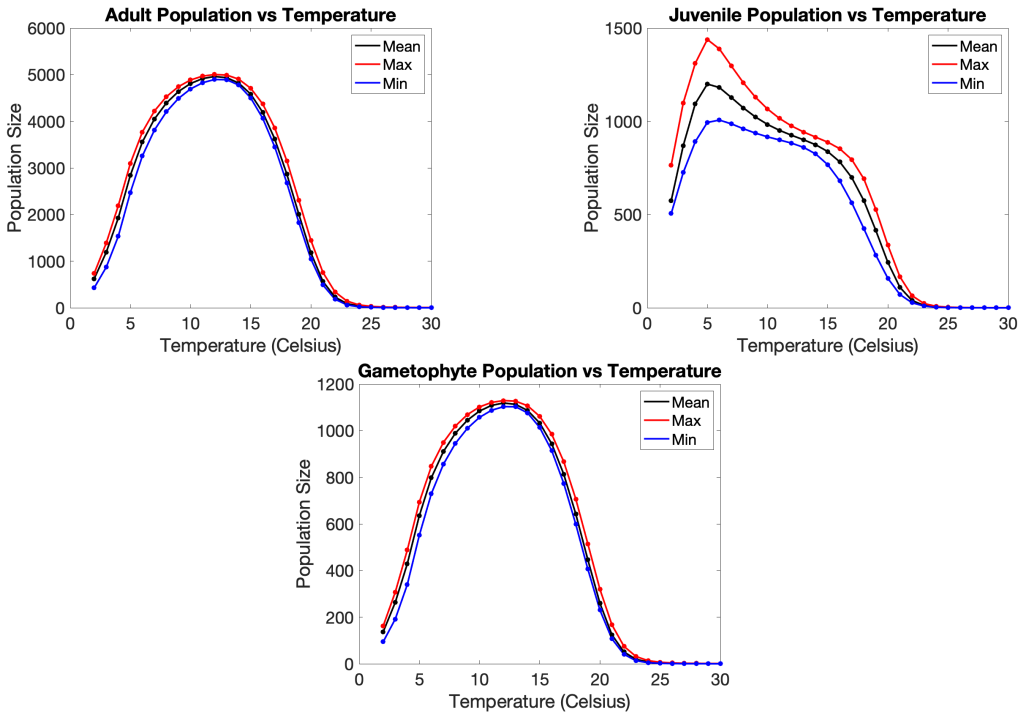

Figure 4: Maximum, mean, and minimum population size after 6 years under various temperature conditions.

Location Based Simulations

For all six location simulations the minimum and maximum temperature were reported along with adult size, and juvenile size for the years 2010 to 2020 (Table 3). The general trend of the table shows that lower latitude locations have higher temperature variation within the 10 years. These lower latitude locations also had larger difference between minimum and maximum population sizes.

Table 3: Simulation results using temperature data from 6 locations along California's coast from 2010 to 2020. Data obtained from *Scripps Institution of Oceanography, University of California San Diego* [31]. † Data from Mendocino was from a separate data source [24].

Location	**Latitude**	**Max Temp °C**	**Min Temp °C**	**Max Adult**	**Min Adult**	**Max Juvenile**	**Min Juvenile**
La Jolla	$32°52.0'N$	26.4	12.5	2990	1208	723	124
San Clemente	$33°25.0'N$	25.5	11.4	3390	1938	779	205
Santa Barbra	$34°24.2'N$	23.4	10.4	4468	2925	879	319
Farallons	$37°18.0'N$	18.0	8.7	4957	4745	962	817
Mendocino †	$39°31.0'N$	17.4044	9.2501	4947	4811	959	840
Trinidad	$41°18.2'N$	18.2	7.5	4938	4850	973	859

Depending on the temperature at each location, we visually observed two distinct behaviors. First, Santa Barbara, San Clemente, and La Jolla which are all located at lower latitudes all experienced highly variable population sizes (Figure 5, top). The populations also began to decrease over during the last five years of the simulation for all three locations. Also, the populations oscillated for the entire simulation. For locations at higher latitudes such as Farallons, Mendocino, and Trinidad, the populations remained relatively constant over the ten year period (Figure 5, bottom).

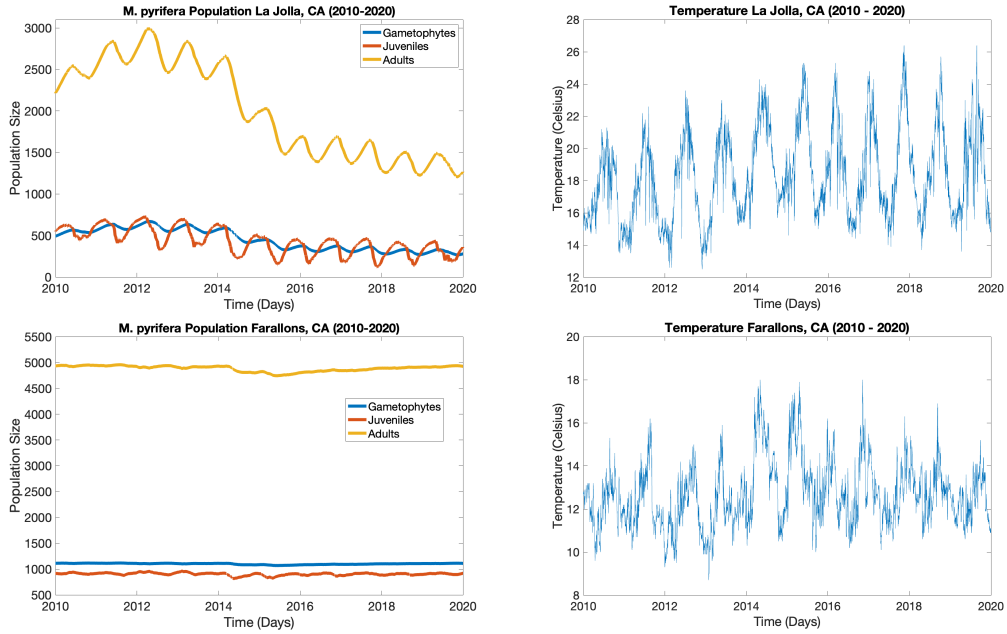

Figure 5: Temporal evolution of *M. pyrifera* populations for 2010 to 2020 (left) for La Jolla, CA and Farallons, CA, and temperature measured at each location during the same period (right).

Future Climate Simulation

Simulating future temperature growth in San Clemente, CA and Trinidad, CA, the *M. pyrifera* population growth is computed for 80 years. In San Clemente, within the 80 year period sea surface temperature remains greater than 24°C for an extended period of time, and adult, juvenile, and gametophyte populations decrease significantly (Figure 7). The adult population decreases due to the increased death rate, δ_A and decreased adult recruitment rate, σ. As a result of lower adult populations, there are less gametophytes produced. Finally the juvenile population has an increased death rate, δ_J.

In Trinidad, the simulated temperature data does not surpass the 21 °C, so the overall population decrease is not as steep compared to the population in San Clemente.

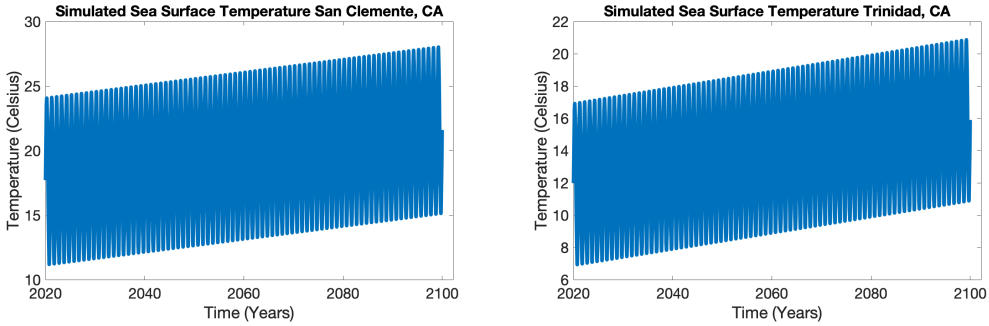

Figure 6: Simulated temperature data from 2020 to 2100 in San Clemente (left) and Trinidad (right).

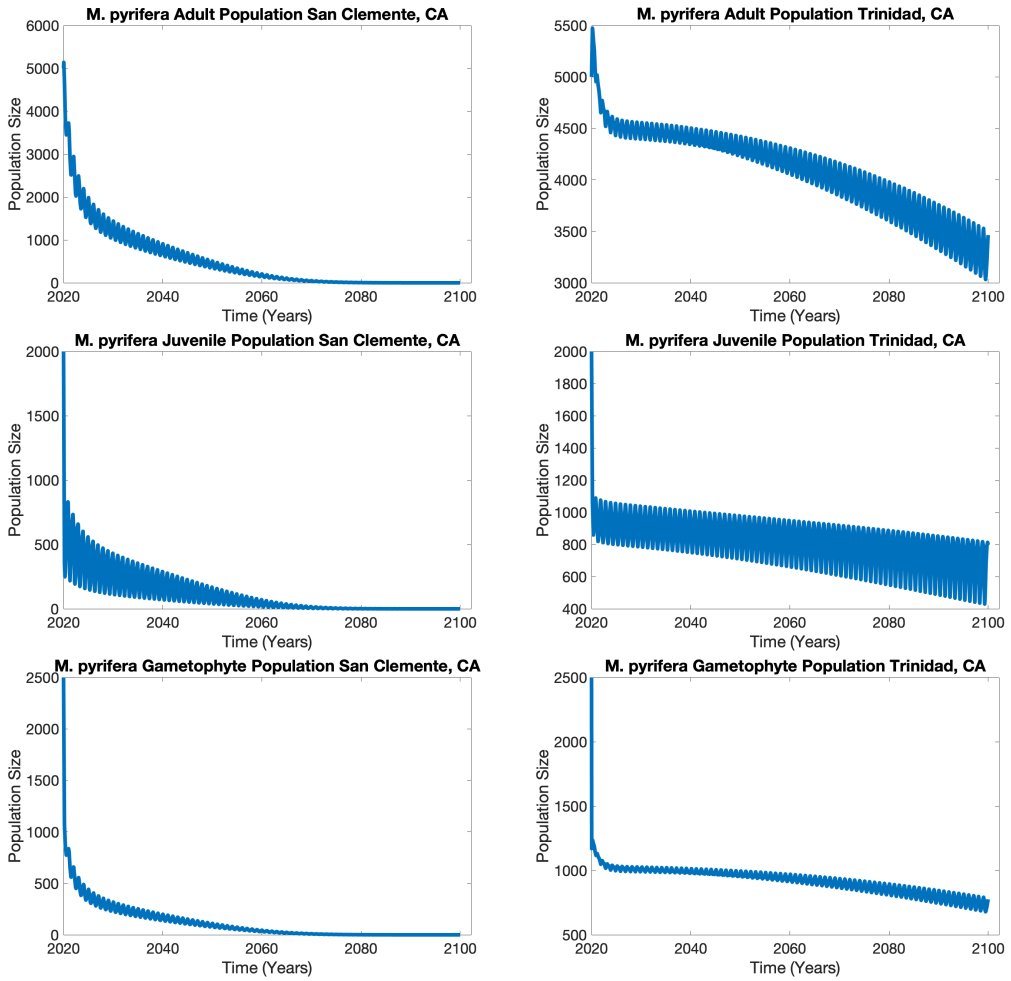

Figure 7: Predicted effect of climate change on adult, juveniles and gametophytes from year 2020 to 2100 in San Clemente, CA (left) and Trinidad, CA (right).

Discussion

This model provided insights into how temperature affects giant kelp. Under conditions of constant temperatures, both juveniles and adult populations do not thrive in high temperatures due to the high death rates and smaller adult recruitment rates (Figure 3). The gametophyte population peaks at the same temperature as the adult population because of the strong correlation between adult and gametophytes and the lack of a temperature dependent gametophyte production rate, β. Because the number of anchored gametophytes is influenced by the competition term, final quantity population size of gametophytes is lower than adults. However, the juveniles did not follow the same trend as the gametophytes and adults. Due to the presence of juvenile recruitment rate, γ, and the juvenile death rate, δ_J, the juvenile population size peaked at approximately 5°C. The juvenile recruitment rate, γ, increased when adult density are small so more gametophytes

can grow to juveniles. Additionally, less juveniles will die at lower temperatures because $\delta_J \approx \delta_{Jmin}$. Adding interannual temporal variation (Figure 4) does not significantly change the mean gametophyte, juvenile, or adult population.

To predict the effects of local climates on the *M. pyrifera*, we gathered temperature data off the coast of California, compared various simulations, and analyzed the results. The results in Table 3 indicate that the temperatures at northern locations did not exceed 24°C in the past 10 years, while two out of the three southern locations did surpass 24°C which generated higher death rates and lower adult recruitment rates. Thus, we can expect that southern locations are more susceptible to rising temperatures compared to the northern ones. Additionally, the results suggest that the southern locations experience a larger range of temperatures throughout the year which makes the population oscillate (Figure 5). The main reason giant kelp populations did not completely die off after exposure to high temperatures is because it has the potential to quickly recover after experiencing high temperatures. An overall summary of these results indicate that population sizes increased with latitude, and southern kelp beds are more at risk of extinction if temperatures continue to rise.

Finally, the predicted effects of climate change in San Clemente, CA and Trinidad, CA on *M. pyrifera* were elucidated in Figure 7. With temperatures rising by 4°C during the 80 year period, fewer juveniles became adults and more adults juveniles died. With the decreasing adult population size, fewer gametophytes in turn are produced. Additionally, due to the low density of adult sporophytes, not enough gametophytes are recruited to juvenile sporophytes thus limiting the total population of giant kelp. In San Clemente, by the year 2080, the remaining population consisted of approximately 1 adult, 2 juveniles and 6 gametophytes. The severe depletion of population indicates that by 2100, if the temperature increases as indicated by the simulated data, the population in San Clemente CA will become extinct. Alternatively, in Trinidad, the increasing temperature does not have as detrimental of an impact on the giant kelp populations. By 2100, a notable proportion of the giant kelp population will still be thriving. This is due, in part, to lower temperatures in the upper latitudes.

Limitations

To model the influence on climate change, our model focus solely on temperature and irradiance within a single giant kelp population. Thus, our model does not take into consideration interspecific competition, pH changes, water depth, and other factors that may affect the giant kelp population.

Additionally, the model does not capture the occurrence of self-fertilization. Male and female gametophytes from the same parent sporophyte are able to fertilize each other [32]. However, the reproductive fitness of these self-fertilized individuals is much lower due to the lack of genetic diversity. They are less resilient and could be more susceptible to higher temperatures than individuals with higher genetic diversity.

Conversely, populations of giant kelp are locally adapted to temperature change [19]. These locally adapted populations can survive higher temperatures and may not display the behavior that was predicted in the results. Instead, location specific parameters could demonstrate local adaption. As of now, our model does not

factor in multiple kelp beds and is fixed at a single average size. Likewise, our model also assumes average size and a constant ocean depth for the kelp beds. However, kelp beds sizes are influenced based on their environment and can reach sizes much smaller or larger. Depending on the location, kelp beds lengths can be anywhere from 7m to 54m [35, 36].

Another limitation is the lack of research on the mortality and lifespan of *M. pyrifera*. Most resources claim that the lifespan of giant kelp is about 4 to 7 years [27, 36]. Others note that the giant kelp's lifespan is about 2 years during the El Niño events or when faced with massive heat waves [14, 17]. There are also locations that are known to have frequent storm events which greatly decrease the lifespan of the kelp [12]. However, researchers have yet to come up with a threshold or maximum age.

In order to fully understand the relationship between adult mortality and temperature, there needs to be a wider range of temperatures tested. Surface temperature and bottom temperature are both crucial in order to fully analyze giant kelp's survival rates. Studies on the effect of surface and bottom temperature would further improve understanding of the effect of temperature on *M. pyrifera*.

Lastly, the abiotic factor irradiance directly affects the growth rate of gametophytes in the model. As the density of adults increases, the sunlight reaching the substrate where the gametophytes are growing is reduced. While irradiance is significantly affected by the quantity of adult sporophytes, other factors such as cloud cover, pollution, time of year, and water depth also impact irradiance but, for simplicity, are not included in the model [5].

Future Steps

Studies indicate that giant kelp have the ability to adapt to different environmental conditions as these organisms are found around the world [21]. By including local adaptation, in terms of latitude, the model would be able to better predict how *M. pyrifera* populations along the coast of California will be affected by climate change. The inclusion of self-fertilization amongst *M. pyrifera*, could also gives rise to a more susceptible population. [32]. Thus, future studies may attempt to analyze the behavior of self-fertilized individuals under temperature increases and compare them to those that are not.

Kelp forest supports a large array of organisms. Some of these species include fish, plankton, sea stars and seabirds that live in the *M. pyrifera's* environs. However, there are negatively impacted interactions such as those with sea urchins which consume *M. pyrifera's* holdfast [37]. Like kelp forest, sea urchins can reach extreme heights of population growth. Urchin barrens can consume up to a foot of the kelp forest a day [28]. Adding interspecies can more accurately predict *M. pyrifera's* population influence over interactions.

Future analyses could implement more environmental parameters. Studies indicate that kelp beds vary in size depending on the location and environments [35]. Future work can implement water depths in the model. Additionally, future studies can expand upon pollution, pH, and nutrients. Other outside factors such as storms play a role in the mortality of *M. pyrifera*. Studies show that adults suffer the greatest mortality

rate out of all the stages of *M. pyrifera* [3]. Oppositely, juvenile's growth rate increases due to the exposure of surface light that was once blocked by the adult *M. pyrifera* [35]. Naturally migration of gametophytes between distinct kelp beds occurs [36]. Thus, incorporating the motion of gametophytes both in and outside kelp beds can more accurately describe population growth.

Conclusion

Our research analyzes the effects of climate change on *M. pyrifera*. Using an age-structured population model on female gametophytes, juvenile sporophytes, and adult sporophytes, we were able to simulate the impacts on temperature and irradiance over time. Unlike other models, our model excludes the male gametophyte population, includes competition between adults and juveniles, and incorporates sea surface temperature from the coast of CA. We constructed several scenarios that account for population and temperature over time. Then we evaluated each *M. pyrifera's* life stage over a time interval. Future results predict that *M. pyrifera* will undergo local extinction in San Clemente, CA if temperature continues to rise, but northern locations such as Trinidad can still support the kelp population. The model suggests that the giant kelp population in the south will die off while the geographic range is limited to northern latitudes.

We encourage motivated researchers to explore additional environmental conditions, life cycles, and data sets for *M. pyrifera*. Furthermore, future researchers can implement migration, local adaptation, self-fertilization, species interactions, massive heat waves, and non-fixed kelp beds.

Acknowledgements

We would like to thank Dr. Jay Taylor, Director and Dr. Fabio Milner, Assistant Director of Quantitative Research for the Life and Social Sciences Program (QRLSSP), for giving us the opportunity to participate in this research program. We would also like to thank Coordinator Ms. Sherry Woodley for her efforts in planning and executing the day to day activities of QRLSSP. This research was conducted as part of 2021 QRLSSP at the Simon A. Levin Mathematical,Computational and Modeling Sciences Center (MCMSC) at Arizona State University (ASU). This project has been partially supported by grants from the National Science Foundation (NSF Grant MPS-DMS-1263374and NSF Grant DMS1757968), the National Security Agency (NSA Grant H98230-J8-1-0005), the Office of the President of ASU, and the Office of the Provost of ASU.

References

[1] Daniel M Alongi. The impact of climate change on mangrove forests. *Current Climate Change Reports*, 1(1):30–39, 2015.

[2] Einar K Anderson and WJ North. In situ studies of spore production and dispersal in the giant kelp, macrocystis. In *Proceedings of the Fifth International Seaweed Symposium, Halifax, August 25–28, 1965*, pages 73–86. Elsevier, 1966.

[3] Nur Arafeh-Dalmau, Gabriela Montaño-Moctezuma, José A Martínez, Rodrigo Beas-Luna, David S Schoeman, and Guillermo Torres-Moye. Extreme marine heatwaves alter kelp forest community near its equatorward distribution limit. *Frontiers in Marine Science*, 6:499, 2019.

[4] Mustafa M Aral and Jiabao Guan. Global sea surface temperature and sea level rise estimation with optimal historical time lag data. *Water*, 8(11):519, 2016.

[5] Mohamed Blal, Seyfallah Khelifi, Rachid Dabou, Nordine Sahouane, Abdeldjalil Slimani, Abdelkrim Rouabhia, Abderrezzaq Ziane, Ammar Necaibia, Ahmed Bouraiou, and Boudjemaa Tidjar. A prediction models for estimating global solar radiation and evaluation meteorological effect on solar radiation potential under several weather conditions at the surface of adrar environment. *Measurement*, 152:107348, 2020.

[6] Matthew B Brown, Matthew S Edwards, and Kwang Young Kim. Effects of climate change on the physiology of giant kelp, macrocystis pyrifera, and grazing by purple urchin, strongylocentrotus purpuratus. *Algae*, 29(3):203–215, 2014.

[7] Alejandro H Buschmann, Karina Villegas, Sandra V Pereda, Carolina Camus, José L Kappes, Robinson Altamirano, Luis Vallejos, and María C Hernández-González. Enhancing yield on macrocystis pyrifera (ochrophyta): The effect of gametophytic developmental strategy. *Algal Research*, 52:102124, 2020.

[8] Carolina Camus, Maribel Solas, Camila Martínez, Jaime Vargas, Cristóbal Garcés, Patricia Gil-Kodaka, Lydia B Ladah, Ester A Serrão, and Sylvain Faugeron. Mates matter: Gametophyte kinship recognition and inbreeding in the giant kelp, macrocystis pyrifera (laminariales, phaeophyceae). *Journal of Phycology*, 2021.

[9] Laura T Carney and Matthew S Edwards. Role of nutrient fluctuations and delayed development in gametophyte reproduction by macrocystis pyrifera (phaeophyceae) in southern california 1. *Journal of Phycology*, 46(5):987–996, 2010.

[10] Intergovernmental Panel On Climate Change. Climate change 2007: Impacts, adaptation and vulnerability. *Genebra, Suíça*, 2001.

[11] Paul K Dayton, Mia J Tegner, Peter B Edwards, and Kristin L Riser. Temporal and spatial scales of kelp demography: the role of oceanographic climate. *Ecological Monographs*, 69(2):219–250, 1999.

[12] A Raine Detmer, Robert J Miller, Daniel C Reed, Tom W Bell, Adrian C Stier, and Holly V Moeller. Variation in disturbance to a foundation species structures the dynamics of a benthic reef community. *Ecology*, 102(5):e03304, 2021.

[13] Lawrence E Deysher and Thomas A Dean. In situ recruitment of sporophytes of the giant kelp, macrocystis pyrifera (l.) ca agardh: effects of physical factors. *Journal of experimental marine biology and ecology*, 103(1-3):41–63, 1986.

[14] MS Edwards and Gustavo Hernandez-Carmona. Delayed recovery of giant kelp near its southern range limit in the north pacific following el niño. *Marine Biology*, 147(1):273–279, 2005.

[15] Pamela A Fernández, Juan Diego Gaitán-Espitia, Pablo P Leal, Matthias Schmid, Andrew T Revill, and Catriona L Hurd. Nitrogen sufficiency enhances thermal tolerance in habitat-forming kelp: implications for acclimation under thermal stress. *Scientific reports*, 10(1):1–12, 2020.

[16] Michael H Graham, Julio A Vasquez, and Alejandro H Buschmann. Global ecology of the giant kelp macrocystis: from ecotypes to ecosystems. *Oceanography and Marine Biology*, 45:39, 2007.

[17] Robert S Grove, Karel Zabloudil, Tim Norall, and Lawrence Deysher. Effects of el nino events on natural kelp beds and artificial reefs in southern california. *ICES Journal of Marine Science*, 59(suppl):S330–S337, 2002.

[18] Ove Hoegh-Guldberg, Elvira S Poloczanska, William Skirving, and Sophie Dove. Coral reef ecosystems under climate change and ocean acidification. *Frontiers in Marine Science*, 4:158, 2017.

[19] Jordan A Hollarsmith, Alejandro H Buschmann, Carolina Camus, and Edwin D Grosholz. Varying reproductive success under ocean warming and acidification across giant kelp (macrocystis pyrifera) populations. *Journal of Experimental Marine Biology and Ecology*, 522:151247, 2020.

[20] John Imbrie and John Z Imbrie. Modeling the climatic response to orbital variations. *Science*, 207(4434):943–953, 1980.

[21] Craig R Johnson and Kenneth H Mann. Diversity, patterns of adaptation, and stability of nova scotian kelp beds. *Ecological Monographs*, 58(2):129–154, 1988.

[22] Brian P Kinlan, Michael H Graham, Enric Sala, and Paul K Dayton. Arrested development of giant kelp (macrocystis pyrifera, phaeophyceae) embryonic sporophytes: A mechanism for delayed recruitment in perennial kelps? 1. *Journal of Phycology*, 39(1):47–57, 2003.

[23] Lydia B Ladah and José A Zertuche-González. Survival of microscopic stages of a perennial kelp (macrocystis pyrifera) from the center and the southern extreme of its range in the northern hemisphere after exposure to simulated el niño stress. *Marine Biology*, 152(3):677–686, 2007.

[24] Meredith L McPherson, Dennis JI Finger, Henry F Houskeeper, Tom W Bell, Mark H Carr, Laura Rogers-Bennett, and Raphael M Kudela. Large-scale shift in the structure of a kelp forest ecosystem co-occurs with an epizootic and marine heatwave. *Communications biology*, 4(1):1–9, 2021.

[25] Ahmet Mert, Kürşad Özkan, Özdemir Şentürk, and Mehmet Güvenç Negiz. Changing the potential distribution of turkey oak (quercus cerris l.) under climate change in turkey. *Polish Journal of Environmental Studies*, 25(4):1633–1638, 2016.

[26] Muhammad Nda, Mohd Shalahuddin Adnan, Kabiru Abdullahi Ahmad, Nura Usman, Mohd Adib Mohammad Razi, and Zawawi Daud. A review on the causes, effects and mitigation of climate changes on the environmental aspects. *International Journal of Integrated Engineering*, 10(4), 2018.

[27] RM Nisbet and JR Bence. Alternative dynamic regimes for canopy-forming kelp: a variant on density-vague population regulation. *The American Naturalist*, 134(3):377–408, 1989.

[28] NOAA. Kelp forests - a description. https://sanctuaries.noaa.gov/visit/ecosystems/kelpdesc.html 2020.

[29] WJ North. Review of macrocystis biology. in "biology of economic algae "(i. akatsuka, ed.) pp. 447-527, 1994.

[30] np. Aerial kelp surveys. https://wildlife.ca.gov/Conservation/Marine/Kelp/Aerial-Kelp-Surveys.

[31] np. SCRIPPS Institution of Oceanography: Shore station program. https://shorestations.ucsd.edu/ Accessed: 2021-07-22.

[32] PT Raimondi, DC Reed, B Gaylord, and L Washburn. Effects of self-fertilization in the giant kelp, macrocystis pyrifera. *Ecology*, 85(12):3267–3276, 2004.

[33] Michael Y Roleda, Jaz N Morris, Christina M McGraw, and Catriona L Hurd. Ocean acidification and seaweed reproduction: increased co 2 ameliorates the negative effect of lowered ph on meiospore germination in the giant kelp m acrocystis pyrifera (l aminariales, p haeophyceae). *Global Change Biology*, 18(3):854–864, 2012.

[34] Eva Rothäusler, Iván Gómez, Ulf Karsten, Fadia Tala, and Martin Thiel. Physiological acclimation of floating macrocystis pyrifera to temperature and irradiance ensures long-term persistence at the sea surface at mid-latitudes. *Journal of Experimental Marine Biology and Ecology*, 405(1-2):33–41, 2011.

[35] Mariana Sánchez-Barredo, Jose Miguel Sandoval-Gil, Jose Antonio Zertuche-González, Lydia B Ladah, María Dolores Belando-Torrentes, Rodrigo Beas-Luna, and Alejandro Cabello-Pasini. Effects of heat waves and light deprivation on giant kelp juveniles (macrocystis pyrifera, laminariales, phaeophyceae). *Journal of phycology*, 56(4):880–894, 2020.

[36] David R Schiel and Michael S Foster. *The biology and ecology of giant kelp forests*. University of California Press, 2015.

[37] MJ Tegner, PK Dayton, PB Edwards, and KL Riser. Sea urchin cavitation of giant kelp (macrocystis pyrifera c. agardh) holdfasts and its effects on kelp mortality across a large california forest. *Journal of Experimental Marine Biology and Ecology*, 191(1):83–99, 1995.

[38] Schery Umanzor, Mary Mar Ramírez-García, Jose Miguel Sandoval-Gil, José Antonio Zertuche-González, and Charles Yarish. Photoacclimation and photoprotection of juvenile sporophytes of macrocystis pyrifera (laminariales, phaeophyceae) under high-light conditions during short-term shallow-water cultivation1. *Journal of phycology*, 56(2):380–392, 2020.

[39] BI Van Tussenbroek. Plant and frond dynamics of the giant kelp, macrocystis pyrifera, forming a fringing zone in the falkland islands. *European Journal of Phycology*, 28(3):161–165, 1993.

A Appendix

A.1 Stability Analysis

The nontrivial equilibrium:

$$G^* = \frac{200K\delta_A(\delta_J+\sigma)(\delta_A\delta_G(-2\delta_J-2\sigma)+\gamma(-2\delta_A\delta_J+\beta\sigma-2\delta_A\sigma))}{\beta\gamma^2\sigma(17\delta_A+183\sigma)},$$
$$J^* = \frac{200K\delta_A(\delta_A\delta_G(-2\delta_J-2\sigma)+\gamma(-2\delta_A\delta_J+\beta\sigma-2\delta_A\sigma))}{\beta\gamma\sigma(17\delta_A+183\sigma)},$$
$$A^* = \frac{K\delta_A\delta_G(-400\delta_J-400\sigma)+\gamma(-400\delta_A\delta_J+200\beta\sigma-400\delta_A\sigma)}{\beta\gamma(17\delta_A+183\sigma)}.$$

To analyze the stability of the model we first found the Jacobian as:

$$J(G^*,J^*,A^*) = \begin{bmatrix} a_{11} & a_{12} & a_{13} \\ a_{21} & a_{22} & a_{23} \\ a_{31} & a_{32} & a_{33} \end{bmatrix}$$

where

$a_{11} = \gamma - \delta_G$

$a_{12} = -\frac{\frac{17}{400}(\delta_A\delta_G(-400\delta_J-400\sigma)+\gamma(-400\delta_A\delta_J+200\beta\sigma-400\delta_A\sigma))}{\gamma(17\delta_A+183\sigma)}$

$a_{13} = \frac{1}{\gamma\sigma(0.09\delta_A+\sigma)}(\delta_A\delta_G(0.09\delta_A\delta_J+0.09\delta_A\sigma+2\delta_J\sigma+2\sigma^2)+\gamma(\delta_A^2(0.09\delta_J+0.09\sigma)-0.5\beta\sigma^2+\delta_A\sigma(2\delta_J+2\sigma)))$

$a_{21} = \gamma$

$a_{22} = -\delta_J - \sigma$

$a_{23} = 0$

$a_{31} = 0$

$a_{32} = \sigma$

$a_{33} = -\delta_A$

Following the above definitions here are a_1, a_2, a_3 and $a_1 \times a_2$:

$$a_1 = \gamma + \delta_A + \delta_G + \delta_J + \sigma$$

$$a_2 = \frac{1}{\delta_A + 10.76\sigma}(\delta_A^2(\delta_G + \delta_J + \sigma) + \delta_G\sigma(10.76\delta_J + 10.76\sigma) + \delta_A\sigma(10.76\delta_G + 10.76\delta_J + 10.76\sigma) + \gamma(\delta_A^2 + 10.76\delta_A\sigma + \sigma(0.5\beta + 10.76\delta_J + 10.76\sigma)))$$

$$a_3 = \gamma\delta_A\delta_J + \delta_A\delta_G\delta_J - 0.5\beta\gamma\sigma + \gamma\delta_A\sigma + \delta_A\delta_G\sigma - \frac{2\gamma\delta_A^2\delta_J}{\delta_A + 10.76\sigma} - \frac{2\delta_A^2\delta_G\delta_J}{\delta_A + 10.76\sigma} + \frac{\beta\gamma\delta_A\sigma}{\delta_A + 10.76\sigma} - \frac{2\gamma\delta_A^2\sigma}{\delta_A + 10.76\sigma} - \frac{2\delta_A^2\delta_G\sigma}{\delta_A + 10.76\sigma} - \frac{21.53\gamma\delta_A\delta_J\sigma}{\delta_A + 10.76\sigma} - \frac{21.53\delta_A\delta_G\delta_J\sigma}{\delta_A + 10.76\sigma} + \frac{10.76\beta\gamma\sigma^2}{\delta_A + 10.76\sigma} - \frac{21.53\gamma\delta_A\sigma^2}{\delta_A + 10.76\sigma} - \frac{21.53\delta_A\delta_G\sigma^2}{\delta_A + 10.76\sigma}$$

$$a_1 \times a_2 = \frac{1}{\delta_A + 10.76\sigma}(\gamma + \delta_A + \delta_G + \delta_J + \sigma)(\delta_A^2(\delta_G + \delta_J + \sigma) + \delta_G\sigma(10.76\delta_J + 10.76\sigma) + \delta_G\sigma(10.76\delta_J + 10.76\sigma) + \delta_A\sigma(10.76\delta_G + 10.76\delta_J + 10.76\sigma) + \gamma(\delta_A^2 + 10.76\delta_A\sigma + \sigma(0.5\beta + 10.76\delta_J + 10.76\sigma)))$$

For condition 2 to be met, $a_3 > 0$ implies:

$$0 < \gamma\delta_A\delta_J + \delta_A\delta_G\delta_J - 0.5\beta\gamma\sigma + \gamma\delta_A\sigma + \delta_A\delta_G\sigma - \frac{2\gamma\delta_A^2\delta_J}{\delta_A + 10.76\sigma} - \frac{2\delta_A^2\delta_G\delta_J}{\delta_A + 10.76\sigma} + \frac{\beta\gamma\delta_A\sigma}{\delta_A + 10.76\sigma} - \frac{2\gamma\delta_A^2\sigma}{\delta_A + 10.76\sigma} - \frac{2\delta_A^2\delta_G\sigma}{\delta_A + 10.76\sigma} - \frac{21.53\gamma\delta_A\delta_J\sigma}{\delta_A + 10.76\sigma} - \frac{21.53\delta_A\delta_G\delta_J\sigma}{\delta_A + 10.76\sigma} + \frac{10.76\beta\gamma\sigma^2}{\delta_A + 10.76\sigma} - \frac{21.53\gamma\delta_A\sigma^2}{\delta_A + 10.76\sigma} - \frac{21.53\delta_A\delta_G\sigma^2}{\delta_A + 10.76\sigma}$$

which simplifies to

$$\frac{21.53\gamma\delta_A\sigma^2}{\delta_A + 10.76\sigma} + \frac{21.53\delta_A\delta_G\sigma^2}{\delta_A + 10.76\sigma} + \frac{2\gamma\delta_A^2\sigma}{\delta_A + 10.76\sigma} + \frac{2\delta_A^2\delta_G\sigma}{\delta_A + 10.76\sigma} + \frac{21.53\gamma\delta_A\delta_J\sigma}{\delta_A + 10.76\sigma} + \frac{21.53\delta_A\delta_G\delta_J\sigma}{\delta_A + 10.76\sigma} + \frac{2\gamma\delta_A^2\delta_J}{\delta_A + 10.76\sigma} + \frac{2\delta_A^2\delta_G\delta_J}{\delta_A + 10.76\sigma} + 0.5\beta\gamma\sigma < \gamma\delta_A\delta_J + \delta_A\delta_G\delta_J + \gamma\delta_A\sigma + \delta_A\delta_G\sigma + \frac{\beta\gamma\delta_A\sigma}{\delta_A + 10.76\sigma} + \frac{10.76\beta\gamma\sigma^2}{\delta_A + 10.76\sigma}$$

Finally for condition 3 to be met

$$\frac{a_1 * a_2}{a_3} > 1$$

where a_1, a_2, and a_3 are defined above.

A.2 Matlab Code

```
%sigma/deltaA - temp varied and gamma - irradiance varied

%time
t_span = 1:1:2190;

%initial values for Gametophytes, Juveniles, and Adults
y_init = [40000;15500;15500]; %approx midsized kelp forest

%Parameters
beta = 0.185; %number of gametophytes produced per adult per day
gamma = 0.05; %1/20 days transition from gametophyte to juvenile
sigma = 0.0147; % 1/68 days transition from juvenile to adult
deltaG = 0.3750; %gametophyte death rate
deltaJmax = 0.1640; %max juvenile death rate
deltaJmin = 0.01; %min juvenile death rate
deltaAmax = 0.0045; %max adult death rate
deltaAmin = 0.0027; %min adult death rate
zetaJ = 24; %heaviside variable
zetaA = 24; %heaviside variable
theta = 34254;  %area of space sporophytes occupy in m^2
K = 126867; %carrying capacity

%Temperature Data
 Trinidad_T=csvread('Trinidad_TEMP.csv',32,0,'A33..I17654');
 T_daily = rmmissing(Trinidad_T(13547:17564,6)); %2010 - 2020

%solving the ODE
[T Y] = ode45(@(t,y) kelp_sys(t,y, beta, deltaG, gamma, sigma, deltaJ,deltaJmin, deltaJmax, zetaJ, deltaA,
deltaAmin,deltaAmax,zetaA, K, theta, T_daily),t_span, y_init);

figure
%Plot the population densities against time
plot(T,Y(:,1), 'LineWidth',5);
hold on
plot(T,Y(:,2), 'LineWidth',5);
plot(T,Y(:,3), 'LineWidth',5);
set(gca, 'FontSize',20);
xlabel('Time (Days)');
ylabel('Population Size')
title('Giant Kelp Population Mendocino, CA(2010-2020)');
legend('Gametophytes','Juveniles', 'Adults')
```

```
%Function defining ODE system with extra parameters passed
function dy = kelp_sys(t, y, beta, deltaG, gamma, sigma, deltaJ, deltaJmin, deltaJmax, zetaJ, deltaA,
deltaAmin,deltaAmax,zetaA, K, theta, T_daily)

    G = y(1);
    J = y(2);
    A = y(3);
    A_hat = A/theta; % have theta be 1m^2 (then its a normalized domain)the theta is the area of
    space we are working with.

    t_day = floor(t); % turns into lowest integer

    temp = T_daily(t_day);

    sigma = sigma_fnc(temp); %sigma with respect to temp
    gamma = gamma_fnc(A_hat); %gamma with respect to irradiance
    deltaA = deltaA_fnc(temp); %deltaA with respect to temp
    deltaJ = deltaJ_fnc(temp); %deltaJ with respect to temp

    dG = .5 * beta * A *(1 - ((0.085 * J + 0.915 * A) / K)) - deltaG * (G) - gamma * (G); %Gametophytes
    dJ =  -sigma * J + gamma * (G)- deltaJ * J; %Juveniles
    dA =  sigma * J - deltaA * A; %Adults

    dy = [dG; dJ; dA];
end

function deltaA = deltaA_fnc(T)
    deltaAmax = 0.0045; %max juvenile death rate
    deltaAmin = 0.0027; %min juvenile death rate
    zetaA = 24; %Threshold temperature for adult survival
    deltaA = (deltaAmax - deltaAmin)*(T^10/ (zetaA^10 + T^10)) + deltaAmin; %Hill function
end

function deltaJ = deltaJ_fnc(T)
    deltaJmax = 0.1640; %max juvenile death rate
    deltaJmin = 0.01; %min juvenile death rate
    zetaJ = 24; %Threshold temperature for adult survival
    deltaJ = (deltaJmax - deltaJmin)*(T^10/ (zetaJ^10 + T^10)) + deltaJmin; %Hill function
end

%sigma as a function of temperature
function sigma = sigma_fnc(T)
```

```
    syms x
    %relative growth rate as function of temperature
    RGR = -((T-2).*(T-26))./(36.92 .* 100);
    tval = zeros(1,length(RGR));

    if (RGR > 0 )
        %time it takes for juvenile to become an adult
        for i = 1:length(RGR)
        tval(i) = solve(1 == 0.075*exp((RGR(i))*x),x);
        end
        sigma = max(0,1./tval); %per day
    else
        sigma = 0;
    end
end

%gamma as a function of irradiance
function gamma = gamma_fnc(A_hat)
    k1 = 6.21; %giant kelp  extinction coefficient
    L_S = 1000; %average surface irradiance (Detmer)
    L_B = L_S*exp(-k1*A_hat); %average bottom irradiance via Beer - Lambert Law
    r_G = 5 * 10^(-5); %rate of recruitment of giant kelp gametophytes to juvenile sporophytes
    gamma = r_G * L_B;
end
```